Biochemical Engineering Journal 174 (2021) 108122

Contents lists available at ScienceDirect

Biochemical Engineering Journal

journal homepage: www.elsevier.com/locate/bej

Continuous-mode encapsulation of human stem cell spheroids using droplet-based glass-capillary microfluidic device for 3D bioprinting technology

C.R.S. Mesquita [a,b,1,2], L.E. Charelli [a,b,1,3], L.S. Baptista [c,d,4], C.P. Naveira-Cotta [b,5], T. A. Balbino [a,*,6]

[a] Nanotechnology Engineering Department, Alberto Luiz Coimbra Institute for Graduate Studies and Research in Engineering, Federal University of Rio de Janeiro (UFRJ), Rio de Janeiro, Brazil
[b] Laboratory of Nano, and Microfluidics and Microsystems, LabMEMS, Mechanical Engineering Dept. (PEM), Federal University of Rio de Janeiro (UFRJ), Rio de Janeiro, Brazil
[c] Laboratory of Tissue Bioengineering, National Institute of Metrology, Quality and Technology (Inmetro), Duque de Caxias, Rio de Janeiro, Brazil
[d] Nucleus of Multidisciplinary Research in Biology (Numpex-Bio), Federal University of Rio de Janeiro (UFRJ), Duque de Caxias, Rio de Janeiro, Brazil

ARTICLE INFO

Keywords:
Droplet-based microfluidics
Cell encapsulation
Cellular spheroids
Mesenchymal stem cells
Tissue engineering
Droplet-based bioprinting

ABSTRACT

Droplet-based microfluidics generates droplets with reproducibility, repeatability, and monodispersity, resulting in decreased reaction time with high yield production. Due to its advantages, its technology has been used to encapsulate biologics for cell therapy, biomaterials, and tissue engineering. However, the encapsulation of superior in vitro culture models, such as cellular spheroids is an ongoing challenge. In this work, we present a continuous process for the encapsulation of mesenchymal stem cell spheroids into alginate hydrogel droplets, using a glass-capillary-based microfluidic device. The device geometry comprises co-flow and hydrodynamic focusing techniques, in which two round glass capillaries are aligned inside a square glass capillary. The encapsulated spheroids were composed of human adipose-derived mesenchymal cells (ASCs) with a diameter of 400 μm. The encapsulation of ASC spheroids was performed into single droplets with approximately 600 μm in size, under a total volumetric flow rate of 14 mL h^{-1}. The developed microdevice was able to generate 200 droplets/min. Moreover, they were able to promote the gelation simultaneously with spheroids encapsulation without compromising their morphology. The stability of the droplet was achieved using 10% of surfactant. In addition, encapsulated spheroids were able to be seeded into PLA scaffolds without compromising either the droplet and their morphology. The successful and homogeneous encapsulation of stem cell spheroids has high applicability in forefront regenerative medicine strategies, such as droplet-based bioprinting. Hence, biofabricating physiological relevant tissue-like constructs with cost and time efficiency.

1. Introduction

Cellular spheroids are three-dimensional (3D) micro-tissues models formed by a suspension of cells that underwent self-assembly [1]. Due to their resemblance to the human physiological system, they have been used as predictive study models in several fields such as tissue engineering, drug development, disease modeling, and personalized medicine [2]. Moreover, cellular spheroids composed of mesenchymal stem cells have shown increased regenerative properties as well as pro-angiogenic potential, steadier differentiation, and phenotype [3].

* Corresponding author.
E-mail address: tiagoab@pent.coppe.ufrj.br (T.A. Balbino).
[1] Both authors contributed equally to this work.
[2] ORCID: 0000-0002-5264-7258.
[3] ORCID: 0000-0002-6565-7543.
[4] ORCID: 0000-0001-9998-8044.
[5] ORCID: 0000-0001-8073-5602.
[6] ORCID: 0000-0001-8522-1889.

https://doi.org/10.1016/j.bej.2021.108122
Received 12 November 2020; Received in revised form 25 June 2021; Accepted 28 June 2021
Available online 1 July 2021

Due to their several advantages, coupled with their ability to fuse with each other, cellular spheroids are desirable raw materials for forefront regenerative medicine protocols, ranging from cell therapies to 3D bioprinting [1,4]. For 3D bioprinting protocols, cellular spheroids are mainly used as building blocks to create complex tissue-like constructs with enhanced biological relevance [2,4].

To date, many studies have reported the use of cellular spheroids to biofabricate heterogeneous tissue-like constructs through 3D bioprinting technology [5,6]. Despite the remarkable outcomes, technical drawbacks such as the final size of the construct, the rheology of the bioink, and the total time to bioprinting the construct still impairs researchers worldwide to achieve more complex constructs with similar in vivo histoarchitecture [7].

To overcome these limitations, microfluidic devices have been considered as printheads in bioprinters [8]. Microfluidic devices are miniaturized platforms that have specific flow characteristics that are capable of controlling the formation of multiple emulsions within micron-sized channels [9]. Thus, chemical, biochemical, and mass/heat transfer analysis in segmented flows, such as droplets, within these devices are more efficient due to their dimensional scaling [10]. The droplet-based microfluidic encapsulation of cells promotes a large reduction in the volume of reagents and samples required for the assays, it is cost-effective with high yield production and enables sophisticated fabrication of bioinks for bioprinting [10,11]. Kim et al., in their pioneering work, used droplet-based bioprinting to biofabricate a human diabetic skin model. Through this technique, it was possible to biofabricated a diabetic skin model with epiderm, derm, hypoderm, and vasculature [11].

The encapsulation of cells through microfluidic devices, for bioprinting applications (i.e., lab-on-a-printer), overcome traditional bioprinting challenges. The main advantages of this combination are high precision and speed, low shear stress, microscale resolution as well as the ability to engineer enhanced smart bioinks [12]. Aiming to combine the advantages of microfluidic encapsulation with the potential of cellular spheroids, in this work, we present a simple and reproducible process for the encapsulation of human stem cell spheroids in alginate droplets. The microdevice has 3 inlets and 1 outlet, in which the alginate and calcium chloride co-flow separately forming the microdroplets in the hydrodynamic focus region; corn oil was used as the continuous phase. The process presented herein is a technological alternative to overcome challenges in bioprinting, especially those addressed to the manipulation of Stem cell spheroids and to the controlling of droplet size homogeneity. The advantage of this concept is its gelation occurring at the same time as its encapsulation, allowing adjustment to specific experimental requirements. To the best of our knowledge, it is the first time that the encapsulation of micron-sized cellular spheroids, using glass-capillary-based microfluidic devices, was addressed. The successful and homogeneous encapsulation of stem cell spheroids has high applicability in forefront regenerative medicine strategies, such as droplet-based bioprinting. Hence, biofabricating physiological relevant tissue-like constructs with tissue fidelity.

2. Materials and methods

2.1. Reagents and materials

Corn oil (CO) (acid value ~0.2% - used for continuous phase) was purchased from a local grocery store and stored at room temperature until its use. All chemicals were purchased from Sigma Aldrich Brazil (São Paulo, Brazil). Sodium alginate (Viscosity: 10–25 mPa.s), Calcium chloride (Cacl2), Span 80 (viscosity 1000–2000 mPa.s (20 °C) were obtained from Sigma–Aldrich. All solutions were prepared with deionized water by a water purifier - Gehaka OS10LXE (Gehaka, SP, Bra).

For droplets generation, sodium alginate solutions were prepared from 1% (w/v), 1.5% (w/v) and 2% (w/v). $CaCl_2$ solutions were prepared in various concentrations from 1% by weight to 2% by weight, both were used as dispersed phases. After the optimal choice of alginate and sodium chloride concentrations, the Span 80 continuous phase was added (concentrations of 1%, 2%, 5%, and 10% v/v) as a surfactant to prevent droplet coalescence in the collection chambers. For better observation and imaging, 0.05% (v/v) of food coloring was dispersed in the sodium alginate solution.

2.2. Adipose-derived mesenchymal stem cell (ASC) spheroids formation

For this study, we used cryopreserved human adipose-derived mesenchymal stem cells at passage 2. ASCs were obtained from healthy donors (n = 2) that underwent plastic surgery. The detailed methodology can be seen in [13]. ASCs were thawed and cultured in 150 cm^2 flasks with Chemically Defined Mesenchymal Stem Cell Medium (MSCGM-CDTM-Lonza,Walkersville, MD, USA), supplemented with 2% fetal bovine serum, 100 μg/mL penicillin, and 100 μg/mL streptomycin (Sigma Aldrich, St. Louis, MO, USA), and.

maintained at 37 °C (with 5% of CO_2), for four days until it reached 80% of confluence.

After the monolayer reached 80% of confluence, the cells were harvested with 0.125% of trypsin and 0.78 mM ethylenediamine tetraacetic acid (EDTA) (Gibco-BRL, USA), for 5 min. To form ASC spheroids, the cells suspension was centrifuged at 400 g for 5 min, and 2×10^6 cells in DMEM (supplemented as explicated below) were plated into micromolded non-adhesive hydrogel with 81 circular recesses (2% agarose—UltrapureAgarose, Invitrogen, Waltham, MA, USA—in 0.9% NaCl), according to the manufacturer's recommendations (Microtissue Inc., USA), and incubated for 24 h, at 37 °C and 5% of CO_2, for the formation of one spheroid per circular recess Fig. 1. ASC spheroids were maintained in DMEM low glucose supplemented with 50 μg/mL ascorbic acid (Sigma), 1.25 μg/mL human albumin (Farma Biagini SPA, Castelvecchio Pascoli,Italy), 100 μg/mL penicillin, 100 μg/mL streptomycin (Sigma) and Insulin-Transferrin-Selenium (ITS) (1 X; Lonza), at 37 °C and 5% of CO_2, for 24 h prior to use within the device.

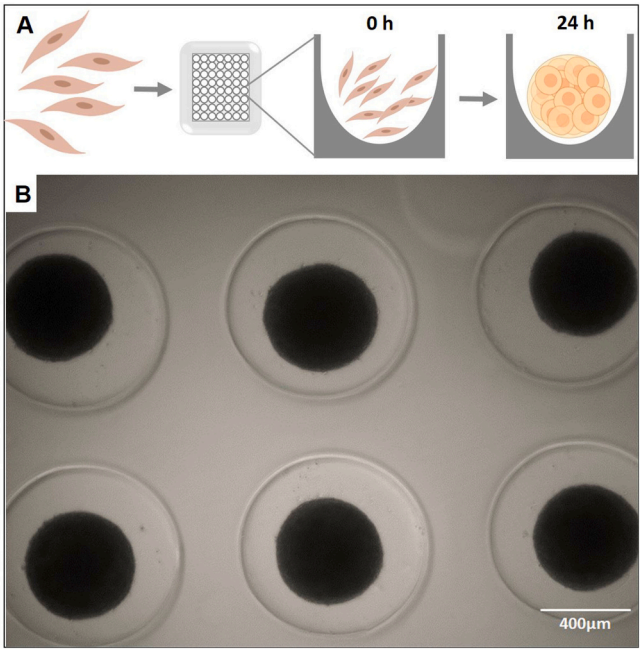

Fig. 1. ASC spheroids formation. (A) Schematic representation of ASC spheroids production. A suspension of 2×10^6 cells is seeded onto a non-adherent hydrogel composed of 81 circular recesses. After 24 h, the ASCs inside the resection underwent self-assembly, resulting in 81 ASC spheroids per mold. (B) Phase-contrast image of ASC spheroids inside the hydrogel. ASC: Adipose-derived mesenchymal stem cells. Scale bar: 400 μm.

2.3. Design of the microfluidic device

The design of the glass capillary device is shown in Fig. 2. The microfluidic device model used in the experiments consisted of two circular section capillaries (WPI - World Precision Instruments, USA - 1000 μm external diameter and 580 μm internal diameter), arranged concentrically inside a rectangular capillary (Vitrocom company, China - external dimensions of 1.05 x 1.05 mm and 600 x 600 μm of internal dimensions). Coaxial alignment was obtained using the internal dimensions of the square capillary (600 μm) approximately similar to the external dimensions of the cylindrical capillaries (580 μm). The three capillaries were fixed with epoxy glue (Araldite®) on a microscope slide (PerfectaLab, Brazil). The injection capillary with a taper of its average internal diameter in the final section of the microchannel, which makes the area through which the internal current passes along the smaller microchannel, in order to obtain greater control in the size of the generated drops. For this, the internal injection capillary was obtained through a Micropipette Extractor (Microelectrode Puller PUL-1000®), where the size of the capillary tip was adjusted to the desired size (approximately 400 μm) using paper and making control of the desired diameter by checking the Hirox Microscope. The mixture between the internal and intermediate currents formed the hydrogel emulsion in the space between the injection and collection capillaries.

2.4. Production of calcium alginate microparticles

To produce the alginate droplets without and with stem cell spheroids, the inlet ports of the cylindrical capillaries and the needles were connected to their respective syringes, which were automatically driven by syringe pumps (NE 1000, New Era Pumping Systems Inc.) (Fig. 2). During the tubing connection, it is important to ensure that there are no air bubbles within the device, this is done through mechanical shocks in the syringes so that all the air can be close to the tip of the syringe, thus obtaining a biphasic mixture, and the plunger is reinforced to remove this air phase until a visually lowering fluid, with a homogeneous characteristic. Otherwise, instability might be observed in the dripping regime for the homogeneous formation of droplets. The formation of emulsions within the microfluidic device was monitored using a 3D digital microscope (Hirox KH-8700, USA) associated with a 1/8-inch digital CCD.

The device comprises three inlet-ports and one out-let port in which the alginate - with or without stem cell spheroids - that constitutes the inner current (Q_{in}) were pumped through the injection round capillary; the inner part of one of the circular capillaries, the fluid that makes up the intermediate current (Q_{mid}) flows through the external capillary in the same direction (co-flow), these currents together formed the dispersed phase (Q_D) flowing in the device. While the fluid that forms the external current (Q_{out}) of the emulsion, also called the continuous phase (Q_C), flows through the external capillary, but in the opposite direction to the other fluids (hydrodynamic focusing). When the three fluids enter the collection capillary, a homogeneous emulsion with its proper gellation perfect emulsion is formed. Initially, the flow rates of the continuous and dispersed phase varied between 7 and 15 mL h^{-1} and 3–7 m Lh^{-1}, respectively. For droplet generation, to confirm the gelation process of the microdroplets, sodium alginate solutions were prepared from 1% (wt/v), 1.5% (wt/v) and 2% (wt/v). $CaCl_2$ solutions were prepared in various concentrations from 1% by weight to 2% by weight, both were used as the dispersed phase. After the optimal choice of alginate and sodium chloride concentrations, the Span 80 continuous phase was added (concentrations of 1%, 2%, 5%, and 10% v/v) as a surfactant to prevent droplets coalescence in the collection chambers. For better observation and imaging, 0.05% (v/v) of food coloring was dispersed in the sodium alginate solution. For the encapsulation of stem cell spheroids n = 30.

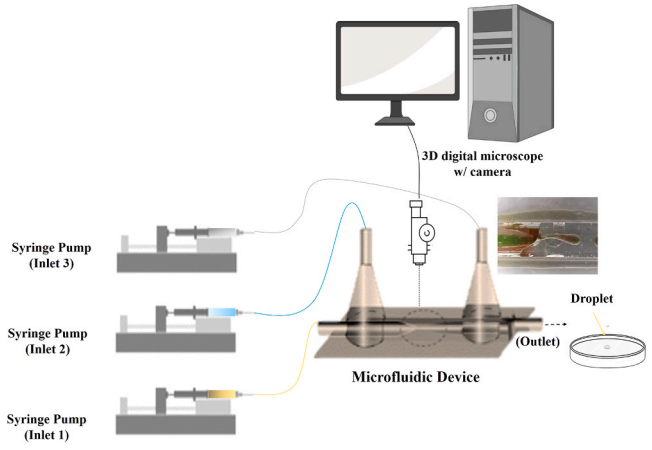

Fig. 2. Schematic representation of the experimental assembly. The microfluidic device is placed over the microscope stage. The needles are connected to the syringes and placed on the pumps, through rubber hoses. Real-time records are made through the camera attached to the microscope.

2.5. Size control

After analyzing the flow regime of the different arrangements, all droplets generated through a 3D digital microscope (Hirox KH-8700, USA) associated with a 1/8-inch digital CCD camera were characterized. Each droplet had its diameter measured in a sample of approximately 120 microdroplets being evaluated for each relationship between the internal, intermediate, and external currents measured. Among those droplets, 30 droplets were separated for statistical analysis, in which the results were parameterized to evaluate the size of the generated microdroplets.

2.6. Statistical analysis

Numerical data are reported as expanded uncertainty using the STATISTICA® - StatSoft, in which the One-way ANOVA analysis with the quick specs dialog method was used. Where $P < 0.05$ was considered significant, 30 droplets were analyzed in triplicate.

3. Results and discussion

3.1. The droplet-based glass-capillary microfluidic device produced monodisperse and stable droplets

A droplet-based glass-capillary microfluidic device combining hydrodynamic focusing and co-flow geometry was developed (Fig. 3 A and B). In order to regulate the generation of microdroplets produced by the device, we investigated the influence of fluid flow rates on the droplet diameter. For the initial conditions, no surfactant was used. The formation of droplets started when the sum of the flows of the continuous phases equaled or exceeded the dispersion $\Sigma Q_D > Q_C$, with the generation of droplets stable (dripping). However, when the flow rate of the continuous phase (Q_{out}) was between 4 and 9 mLh^{-1}, and its ratio was less than 1, larger and unstable droplets (squeezing) were generated. The stable droplets (dripping regime) were achieved when the flow of the continuous phase increased. Moreover, in a condition of $Q_C \gg Q_D$ or $Q_D \gg Q_C$ extreme values of ratios are obtained, $R < 0.5$ and $R \geq 2$, and the drop breaking process does not occur (Fig. 3C).

The dripping and jetting mechanisms are closely related, and the transition between them is induced by the variation in the flow of the external fluid Q_{out}. The relationship between the ratio of the generated drop radius, R_{drop}, to the injection capillary radius, R_{capinj}, and the ratio of the dispersed phases (Q_D) to the continuous phase (Q_C) can be seen in Fig. 3D. The radius of the droplets, R_{drop}, decreased linearly with Q_{out} (Fig. 3D, blue squares). In the jetting regime, where we have increased

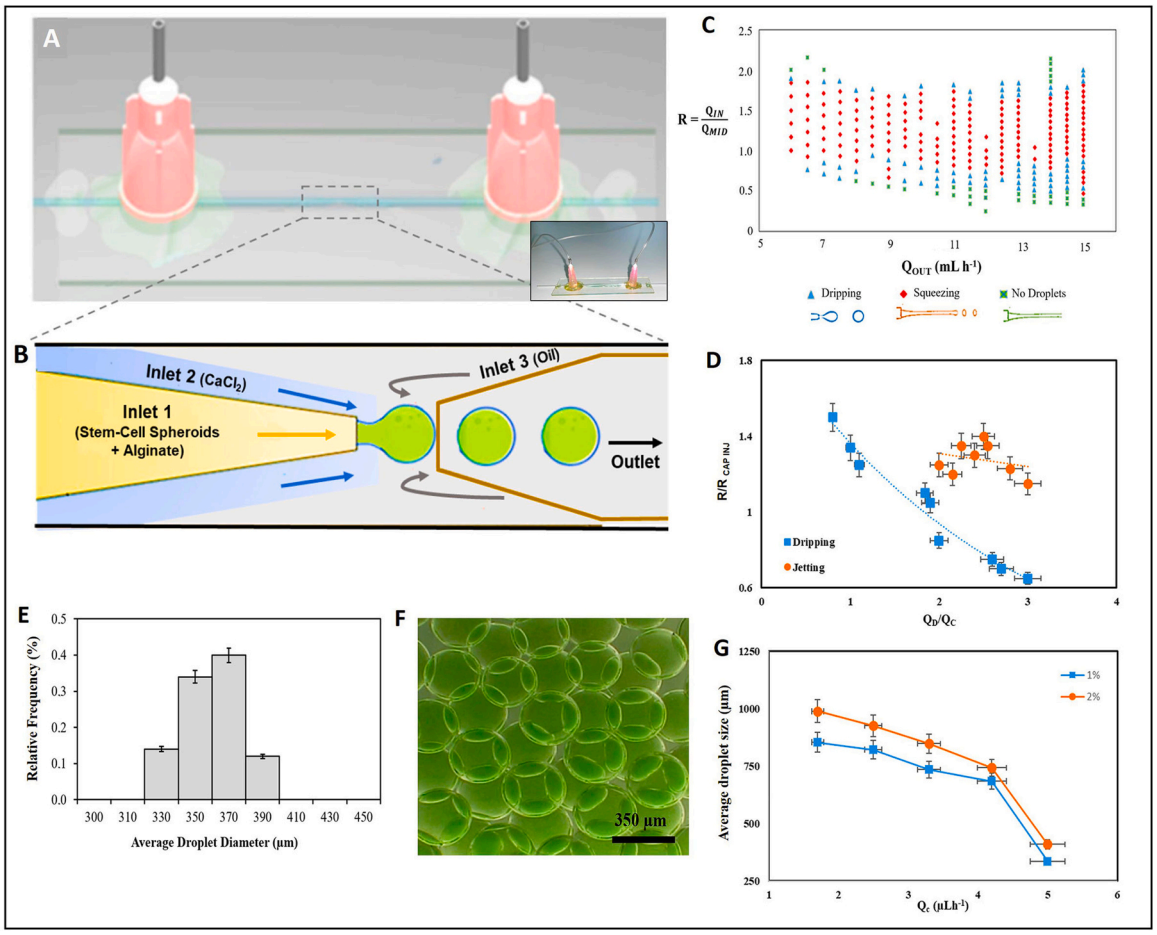

Fig. 3. The droplet formation process. (A) Schematic illustration of the glass capillary microfluidic device. Insert: Droplet-based glass-capillary microfluidic device. (B) A detailed view of the two conical cylindrical glass capillaries is inserted in a square capillary to produce single water-in-oil droplets with corn oil as the continuous phase, and sodium alginate and calcium chloride as the dispersed phase. (C) Diagram of droplet formation as a function of the flow rate ratio ($R = Q_{IN}/Q_{MID}$) between alginate, cross-linker streams, and the stream-flow rate of the continuous phase (Q_{OUT}). (D) The ratio between droplet radius and injection capillary radius versus dispersed and continuous flow-rates ratio. The blue squares and orange circle dots represent the drop diameter in the dripping and jetting regimes, respectively. The blue dotted line represents the drop size trend line in the dripping regime, and the orange dotted line represents the drop size in the jetting regime. Data expressed as Mean ± 0.1, n = 120, $P < 0.05$. (E-F) Droplet diameter size distribution and morphology of the droplets produced under conditions according to droplet 6 (Table 1), respectively. Scale Bar: 350μm. Data expressed as Mean ± 0.08, n = 120, $P < 0.05$. (G) Average droplet size as a function of the continuous phase flow rate at two different concentrations of alginate (1% and 2%). Data expressed as Mean ± 48.4, n = 120, $P < 0.05$. (For interpretation of the references to colour in this figure legend, the reader is referred to the web version of this article.)

the flow rate of the dispersed phase (Qout), and consequently the values of this Q_D/Q_c ratio increased between 2 and 3, we observe a discontinuity in the values found (Fig. 3D, orange circles). Unlike the dripping regime, where it is possible to notice a trend occurring. When the R/R_{capinj} ratio decreases, the Q_D/Q_c ratio increases. From this relationship, it was possible to define two parameters: The flow regime to be studied - dripping regime, due to its predictable behavior, as shown in Fig. 3C (blue squares), and by analyzing the flows and regime generated in Fig. 3C, and consequently, their average diameters, we could define the diameter of the injection capillary. In this way, the geometry of glass capillaries has a ratio close to 1 between the flow rates of the continuous and dispersed phases, stabilizing their flow, and presenting a more stable droplet generation profile.

From the analysis of the flow regime of the different arrangements shown in Fig. 3D, six droplets of the dripping regime were chosen to be further analyzed, as summarized in Table 1. As shown in Table 1, the

Table 1
Droplets studied for evaluation between the dispersed (Q_{out}) and continuous (Q_{in} and Q_{mid}) phases correlating with the average drop size generated. The average drop size and CV were obtained from 30 droplets analyzed in triplicate.

Droplets	Inner stream (Qin) (mLh^{-1})	Middle stream (Qmid) (mLh^{-1})	Outer stream (Qout) (mLh^{-1})	Ratio between phases Phases $\frac{Qin + Qmid}{Qout}$	Average drop size± Expanded uncertainty[a] (μm)	Coefficient of variation
1	3.5	3.5	6.5	1.1	404.1 ± 2	14%
2	3.5	3.5	7	1.0	384.5 ± 2	16%
3	4	4	6	1.3	413.7 ± 3	18%
4	4	4	6.5	1.2	344.6 ± 1	9.0%
5	4	4	8	1.0	562.7 ± 3	15%
6	3.5	4.5	6	1.3	356.8 ± 1	8.8%

[a] Considering a confidence level of 95%

coefficient of variation increased while decreasing the ratio between the dispersed and continuous phases. Moreover, when comparing droplets that had the same flows in the dispersed phases, it was seen that the increase in the flow rate of the continuous phase (Q_{out}) decreased the droplet size, droplets 1 and 2 showed this effect, where the diameter of the microdroplets decreased from 404.1 ± 5 μm to 384.5 ± 6 μm, and in droplets 3 and 4, the diameter of the microdroplets decreased from 413.7 ± 7 μm to 344.6 ± 3 μm. The droplet size increases with the increasing flow rate of the dispersed phase and decreases with the increasing flow rate of the continuous phase.

Then we varied the flow rates of the Q_{in} and Q_{mid} phases and the oil flow (Q_{out}) was fixed, according to droplets 1 and 4. The results are shown in Table 1. It can be seen that when the oil phase increased and the phases Q_{in} and Q_{mid} decreased, the droplets became larger. When the flow rates of the Q_{in} and Q_{mid} phases increased from 3.5 to 4.0 mL h^{-1}, the droplets decreased from about 404.1 ± 5 – 344.6 ± 3 μm.

After the analysis of the tests, shown in Fig. 3D, it was observed that the region of formation of stable drops had values of the ratio between the continuous and dispersed phases in the range between 1.1 and 1.7. Analyzing the main studied droplets shown in Fig. 3C, it was possible to see that droplets 4 and 6 respectively, for having flows of internal currents (4/3.5 mL h^{-1}), intermediate (4/4.5 mL h^{-1}), and external (6.5/7 mL h^{-1}) and approximately similar phase-to-phase ratio (1.2/1.3) were excellent droplets to continue with the study. It is important to highlight the lower polydispersity of droplets 6 when compared to the other droplets, with droplets with an average size 356.9 ± 4 μm being generated with a greater polydispersity (but still less than 5%), indicated by a coefficient of variation (CV) equal to 8.8%, as shown in Fig. 3E and F.

According to Fig. 3G, the concentration of 1% alginate was more advantageous compared to the average droplet size, due to spheroid diameters (values ranging from 300 to 400 μm). Accordingly, as previously reported, the 2% alginate solution even generating droplets for a certain time was not as viable since it obstructs the device and, consequently, makes it inoperable. It is important to highlight that the 1.5% alginate concentration was also used for this analysis, however, the channel obstruction remained occurring as well as using the 2% concentrations, the main difference was the time for the microchannel obstruction that follows a direct relationship: The higher the concentration of alginate, the shorter the time to obstruct the microchannel.

In this work, the droplet-based glass-capillary microfluidic device was developed combining hydrodynamic focusing and co-flow geometry. The strategy reported in this work enables the gelation to occur at the same time as the encapsulation, which allows adjustments to specific experimental requirements.

Droplet-based microfluidics allows the manipulation of small fluid packages, in the form of microdroplets, that promote several advantages for biological assays [14]. In these systems, one is able to achieve a significant decrease in the volume of required reagents, as well as a decrease in reaction time, and high yield production in a cost-effective manner, without labor-intensive experiments [15]. Moreover, compared with the batch production of droplets, microfluidic devices can generate products with higher monodispersity [14]. Due to their advantages, they are promising devices to be used for regenerative medicine, tissue engineering, and biotechnological applications. The generation of tumor spheroids using a droplet-based microfluidic device was reported by Lee et al. [16]. The authors were able to modulate the final size of the spheroids between 100 and 130 μm with generation frequencies of 70 Hz. The droplets were capable of generating the spheroids, maintaining their morphology and viability, with minimal manual handling [16]. The development of strategies to successfully encapsulate biologics is of paramount significance to use them as delivery systems as well as bioinks in bioprinting protocols [17].

3.2. The successful encapsulation of stem cell spheroids was dependent on the surfactant concentration

We measured the size of the microdroplets produced as a function of Q_c, according to the different surfactant concentrations (Span 80) in the continuous phase (corn oil). In the absence of a surfactant, it was noticed that the generated droplets coalesced at a high frequency, almost instantly. A non-ionic surfactant, sorbitan monooleate (Span 80), was added to the continuous phase which facilitated the formation of microdroplets and avoided subsequent coalescence before gelation. As expected, the diameter of the microdroplets decreased and increased the surfactant concentration in the continuous phase (Fig. 4A–D). Thus, the size of the microdroplets was critically dependent on the concentration of surfactant added to the corn oil.

Fig. 4D shows the effect of the surfactant concentration and the different flow rate of the continuous phase, both at a flow rate of the continuous phase fixed (6.0 μL h^{-1}) of the aqueous phase and a concentration that varies between 1% and 10% of surfactant in the size of the microspheres produced. The average size of the microspheres was dependent on the surfactant concentration, which varied from 335 ± 1 – 733 ± 15 μm, respectively for a variation of Span 80 of 1% and 10%. Therefore, the size of the microdroplets was controlled by varying the surfactant concentration to the continuous phase. The concentration of 10% Span 80 was used, as it was the best event held where we obtained the smallest average drop diameter (Fig. 4C, supplementary movie1). Furthermore, we assessed that the stability of the droplets (i.e., absence of coalescence) was maintained from the formation until the collection microtube (1 m distance from emulsion formation to collection tube).

These microdroplets were observed and evaluated during the period before droplet coalescence (Fig. 4E). This phenomenon occurs after the discharge of the droplets in the collection container and can vary according to the concentration of the surfactant used. In this work, for concentrations of 1%, 2% and 5% the coalescence occurred in less than 1 min, while in the 10% concentration the coalescence occurred in more than two minutes, as seen in Fig. 4E.

Supplementary material related to this article can be found online at doi:10.1016/j.bej.2021.108122.

Thus, the presence of the surfactant slows down the agglutination of the hydrogel microdroplets. In which, during the average period for concentrations of 10%, 5%, 2%, and 1%, observed in Fig. 4E, they were 02 min, 18 s, 48 s, 33 s, and 26 s, respectively. However, the droplets remain intact and the increased concentration of the surfactant leads to a decrease in diameter and an increase in the time before they adhere. It is important to inform that in the absence of the surfactant, that droplet coalescence occurs inside the device, reaching the collection container of already agglutinated droplets.

Alginate microspheres allow the diffusion of nutrients and waste to and from cells, respectively [18]. This polymer has many advantages that make it one of the most used hydrogels in cellular microencapsulation [19], one of them is to form a gel under certain conditions that are suitable for providing long-term cell viability [18].

Since they resemble the natural extracellular matrix, alginate hydrogels can also be used in tissue engineering [18,19] in the encapsulation of transplanted cells; which, in turn, provides an immune isolation barrier for cells and potentially allowing transplantation without the need for immunosuppression [20]. Accordingly, hydrogels composed of alginate have been extensively used in traditional and groundbreaking bioprinting protocols [21].

Alginate droplets can act as three-dimensional micrometric culture units, which allows individual cells and their spheroidal aggregates to be independently monitored and/or manipulated, for example, to deliver cells to repair damaged tissues [18–20]. Nonetheless, the ideal alginate microparticles for the applications aforementioned must be composed of a homogeneous crosslinking and surfactant in concentration that allows stable trapping of the encapsulated cells [21].

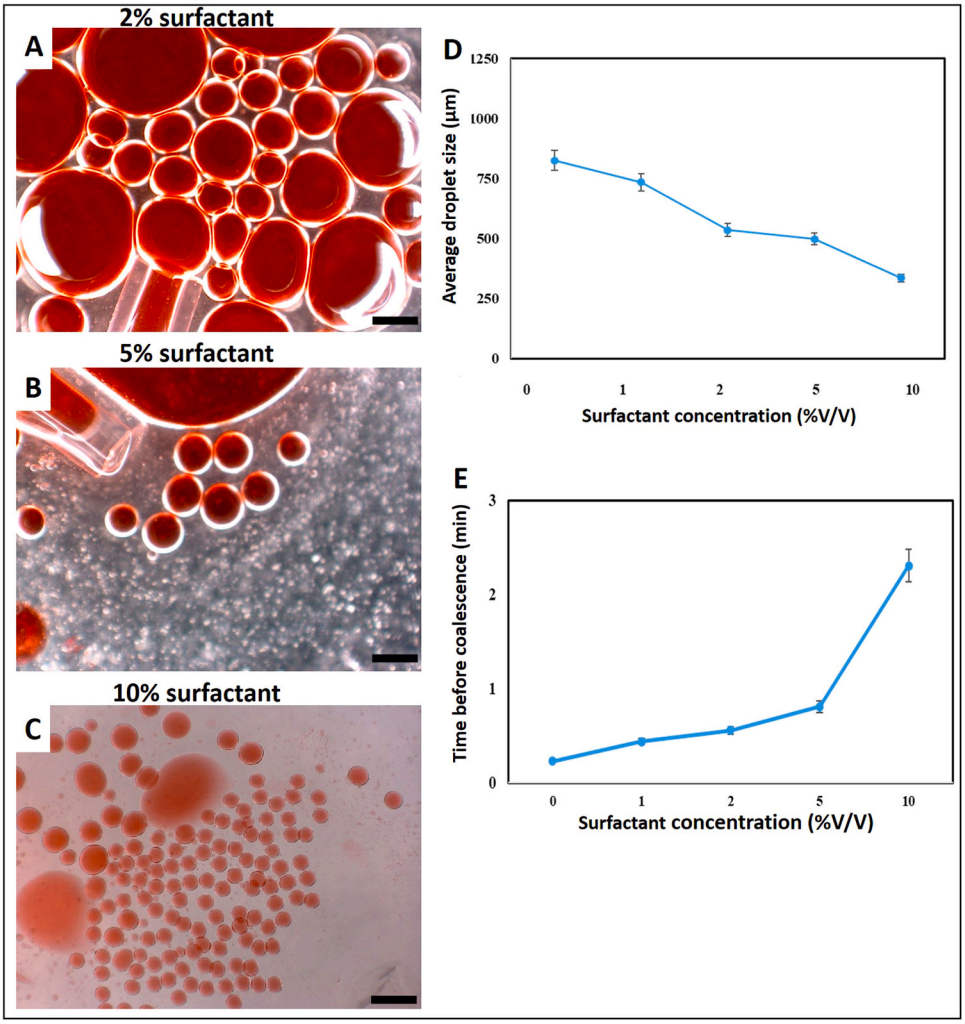

Fig. 4. Effect of surfactant concentration on droplet formation. (A–C) Generated droplets with 2%, 5%, and 10% of surfactant. (D) Dependence on the size of the microdroplets. Data expressed as Mean ± 42.8, 30 droplets were analyzed in triplicate, and (E) Physical stability of alginate microdroplets under different concentrations of surfactant (span 80) produced at a flow rate of the continuous phase (Qc) of 6.0 µL h^{-1}. Data expressed as Mean ± 0.1, $P < 0.05$. 30 droplets were analyzed in triplicate. Scale bar: 400 µm.

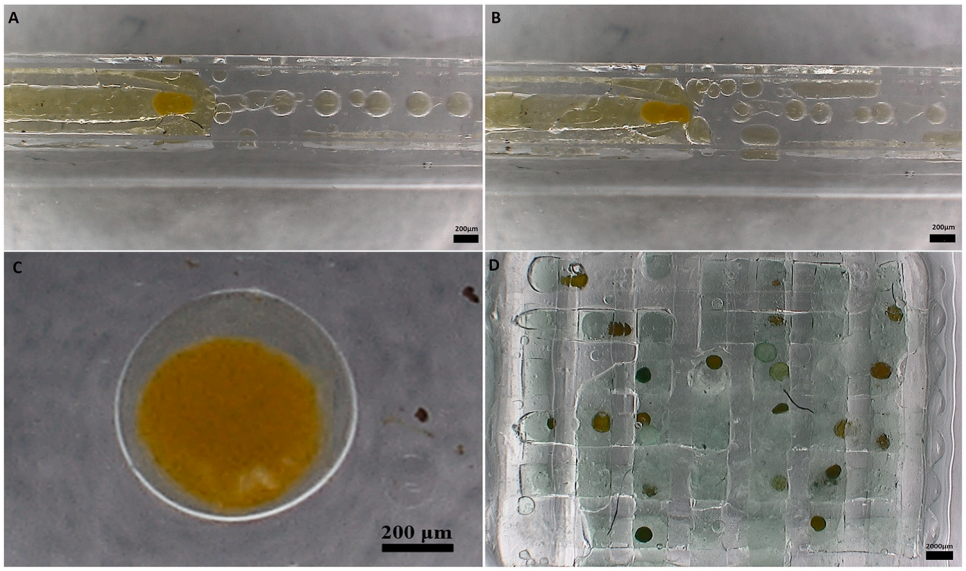

Fig. 5. Encapsulation of stem cell spheroids. (A–C) Individual spheroid encapsulation performed with the flow rates of the internal, intermediate, and external currents of 3.5 mL h^{-1}, 4.5 mL h^{-1}, and 6.0 mL h^{-1}, respectively. Scale Bar: 200 µm. (D) Encapsulated spheroids (green and yellow) seeded in PLA scaffolds (n = 30). Scale Bar: 2000 µm. (For interpretation of the references to colour in this figure legend, the reader is referred to the web version of this article.)

3.3. The continuous mode encapsulation of stem cell spheroids was achieved successfully by using droplet-based glass-capillary microfluidics

Human stem cell spheroids were collected from micromolded non-adhesive hydrogel and suspended in alginate solution for the encapsulation process. While the droplets were flowing along the gelation channel, the mixing between $CaCl_2$ and alginate allowed the gelation processes to occur by the formation of hydrogel granules, due to the chelation between Ca_2^+ and alginate (Fig. 3A and B).

The encapsulation process follows the Poisson statistic. The production of droplets encapsulating individual spheroids is shown in Fig. 5A–C, where the flow rates of the internal, intermediate, and external currents were 3.5, 4.5, and 6.0 mL h^{-1}, respectively. Stem cell spheroids have applications in several areas, ranging from drug development to regenerative medicine and tissue engineering. It is known that stem cell spheroids have augmented capability of differentiation, secretion of pro-angiogenic factors as well as immunomodulation properties [1,2]. Hence, they have been used as building blocks for the biofabrication of physiological relevant tissue-like constructs [2]. To date, 3D bioprinting is one of the most forefront technologies capable of controlling the space-temporal deposition of living cells, biomaterials, and biomolecules [22,23]. The combination of cellular spheroids and 3D bioprinting bridge the gap toward the creation of superior in vitro models and - in the latter future - for organ production [7,24].

Despite the advantages of this combination, the bioprinting of cellular spheroids is still in its infancy, due to the technical challenge that is to produce a bioink able to support its weight (they present high cell density) [7]. Strategies that consist of placing the spheroids into needles have been used, nonetheless, they limit the final morphology of the construct to a tubular form [4]. In this study, we were able to develop a methodology capable of continuously encapsulating stem cell spheroids in a scaffold-free manner. Thus, our microfluidic process may be used as a bioprinting nozzle, depositing spheroids in a free and desirable structure without shear stress, while maintaining the cells viable.

After encapsulation, the encapsulated stem cell spheroids were then seeded into a PLA scaffold (Fig. 5B). We used a PLA scaffold to evaluate whether the droplet containing the spheroids would be placed correctly into the porous of the scaffold as well as maintaining the droplet structure. Our results showed that the droplets containing the stem cell spheroids were successfully seeded into the porous of the scaffold without compromising the spheroid's morphology. It is known that PLA has been used as raw material to compose scaffolds for tissue engineering [25,26]. Thus, testing the integrity of the encapsulated spheroids within these scaffolds are important. The combination between PLA scaffolds and encapsulated spheroids is a promising approach to achieve macro-scale biofabrication. In this scaffold-based strategy, the scaffolds provide a steadier mold for the spheroids to fuse with each other and to form larger tissue [2].

Analyzing the effect of the surfactant on the encapsulated spheroids, it was noticed that the spheroid droplets remained stable for the same time as the empty drops previously described. Nonetheless, after the stability period, the agglutination of the droplets with spheroids occurred (Supplementary Fig. 1), this indicated that other surfactant compositions might be tested to improve the stability of the droplets.

4. Conclusion

We present a microfluidic system based on two different types of geometry, co-flow and hydrodynamic focusing techniques and, therefore, highly flexible, which combines different devices to encapsulate, and manipulate individual spheroids in small drops, allowing the concentrations of secreted molecules to reach detectable levels quickly. The advantage of this concept is its gelation occurring at the same time as its encapsulation, allowing adjustment to specific experimental requirements. The microdroplet generation process was achieved with robustness, repeatability, and yield time. The effective encapsulation of spheroids displays a pivotal role to generate steadier tissue-like constructs i.e., building blocks, that can be used as bioink for bioprinting applications.

CRediT authorship contribution statement

C.R.S Mesquita: Conceptualization, Methodology, Investigation, Formal analysis, Writing - original draft. **L. E. Charelli:** Conceptualization, Methodology, Investigation, Formal analysis, Writing - original draft. **L.S. Baptista:** Conceptualization, Resources, Writing - review & editing, Funding acquisition. **C.P. Naveira-Cotta:** Conceptualization, Methodology, Writing - review & editing, Supervision, Funding acquisition. **T.A. Balbino:** Conceptualization, Methodology, Writing - review & editing, Visualization, Supervision, Funding acquisition.

Declaration of Competing Interest

The authors declare that they have no known competing financial interests or personal relationships that could have appeared to influence the work reported in this paper.

Acknowledgements

This work was partially funded by the National Council for Scientific and Technological Development (CNPq) through national Grant, and also by the Carlos Chagas Filho Foundation for Research Support of the State of Rio de Janeiro (FAPERJ) through state Grant Young Scientist of our State. We thank the National Institute of Metrology, Quality and Technology (INMETRO, RJ, Brazil) and the Nucleus of Multidisciplinary Research in Biology (Numpex-Bio, Federal University of Rio de Janeiro, RJ, Brazil) for the use of their facilities.

Appendix A. Supporting information

Supplementary data associated with this article can be found in the online version at doi:10.1016/j.bej.2021.108122.

References

[1] S. Kim, E. Kim, M. Yamamoto, H. Park, H. Shin, Engineering multi-cellular spheroids for tissue engineering and regenerative medicine, Adv. Healthc. Mater. 9 (2020), 2000608, https://doi.org/10.1002/adhm.202000608.
[2] M. Laschke, M. Menger, Life is 3D: boosting spheroid function for tissue engineering, Trends Biotechnol. 35 (2017) 133–144, https://doi.org/10.1016/j.tibtech.2016.08.004.
[3] M. Laschke, M. Menger, Spheroids as vascularization units: from angiogenesis research to tissue engineering applications, Biotechnol. Adv. 35 (2017) 782–791, https://doi.org/10.1016/j.biotechadv.2017.07.002.
[4] M. Itoh, K. Nakayama, R. Noguchi, K. Kamohara, K. Furukawa, K. Uchihashi, S. Toda, J. Oyama, K. Node, S. Morita, Correction: scaffold-free tubular tissues created by a Bio-3D printer undergo remodeling and endothelialization when implanted in rat aortae, PLoS One 10 (2015), 0145971, https://doi.org/10.1371/journal.pone.0136681.
[5] A. Daly, M. Davidson, J. Burdick, 3D bioprinting of high cell-density heterogeneous tissue models through spheroid fusion within self-healing hydrogels, Nat. Commun. (2021) 12, https://doi.org/10.1038/s41467-021-21029-2.
[6] T. Jiang, J. Munguia-Lopez, S. Flores-Torres, J. Grant, S. Vijayakumar, A. Leon-Rodriguez, J. Kinsella, Directing the self-assembly of tumour spheroids by bioprinting cellular heterogeneous models within alginate/gelatin hydrogels, Sci. Rep. (2017) 7, https://doi.org/10.1038/s41598-017-04691-9.
[7] V. Mironov, R. Visconti, V. Kasyanov, G. Forgacs, C. Drake, R. Markwald, Organ printing: tissue spheroids as building blocks, Biomaterials 30 (2009) 2164–2174, https://doi.org/10.1016/j.biomaterials.2008.12.084.
[8] C. Richard, A. Neild, V. Cadarso, The emerging role of microfluidics in multi-material 3D bioprinting, Lab Chip 20 (2020) 2044–2056, https://doi.org/10.1039/C9LC01184F.
[9] Y.S. Zhang, A. Arneri, S. Bersini, S.R. Shin, K. Zhu, Z. Goli-Malekabadi, J. Aleman, C. Colosi, F. Busignani, V. Dell'Erba, C. Bishop, T. Shupe, D. Demarchi, M. Moretti, M. Rasponi, M.R. Dokmeci, A. Atala, A. Khademhosseini, Bioprinting 3D microfibrous scaffolds for engineering endothelialized myocardium and heart-on-a-chip, Biomaterials 110 (2016) 45–59, https://doi.org/10.1016/j.biomaterials.2016.09.003.

[10] L. Shang, Y. Cheng, Y. Zhao, Emerging droplet microfluidics, Chem. Rev. 117 (2017) 7964–8040, https://doi.org/10.1021/acs.chemrev.6b00848.
[11] B. Kim, M. Ahn, W. Cho, G. Gao, J. Jang, D. Cho, Engineering of diseased human skin equivalent using 3D cell printing for representing pathophysiological hallmarks of type 2 diabetes in vitro, Biomaterials 272 (2021), 120776, https://doi.org/10.1016/j.biomaterials.2021.120776.
[12] C. Colosi, S. Shin, V. Manoharan, S. Massa, M. Costantini, A. Barbetta, M. Dokmeci, M. Dentini, A. Khademhosseini, Microfluidic bioprinting of heterogeneous 3D tissue constructs using low-viscosity bioink, Adv. Mater. 28 (2015) 677–684, https://doi.org/10.1002/adma.201503310.
[13] L. Charelli, N. Müller, K. Silva, L. Lima, C. Sant'Anna, L. Baptista, Biologically produced silver chloride nanoparticles from B. megaterium modulate interleukin secretion by human adipose stem cell spheroids, Cytotechnology 70 (2018) 1655–1669, https://doi.org/10.1007/s10616-018-0257-x.
[14] M. Nie, S. Takeuchi, Bottom-Up Biofabrication Using Microfluidic Techniques, Biofabrication 10 (2018), 044103, https://doi.org/10.1088/1758-5090/aadef9.
[15] H. Gudapati, M. Dey, I. Ozbolat, A comprehensive review on droplet-based bioprinting: past, present and future, Biomaterials 102 (2016) 20–42, https://doi.org/10.1016/j.biomaterials.2016.06.012.
[16] J. Lee, J. Choi, C. Ahrberg, H. Choi, J. Ha, S. Mun, S. Mo, B. Chung, Generation of tumor spheroids using a droplet-based microfluidic device for photothermal therapy, Microsyst. Nanoeng. (2020) 6, https://doi.org/10.1038/s41378-020-0167-x.
[17] G. Orive, E. Santos, D. Poncelet, R. Hernández, J. Pedraz, L. Wahlberg, P. De Vos, D. Emerich, Cell encapsulation: technical and clinical advances, Trends Pharmacol. Sci. 36 (2015) 537–546, https://doi.org/10.1016/j.tips.2015.05.003.
[18] D. Dhamecha, R. Movsas, U. Sano, J. Menon, Applications of alginate microspheres in therapeutics delivery and cell culture: past, present and future, Int. J. Pharm. 569 (2019), 118627, https://doi.org/10.1016/j.ijpharm.2019.118627.
[19] O. Khanna, J. Larson, M. Moya, E. Opara, E. Brey, Generation of alginate microspheres for biomedical applications, J. Vis. Exp. (2012), https://doi.org/10.3791/3388.
[20] N. Uyen, Z. Abdul Hamid, A. Nurazreena, Fabrication and characterization of alginate microspheres, Mater. Today.: Proc. 17 (2019) 792–797, https://doi.org/10.1016/j.matpr.2019.06.364.
[21] Y. Zhang, P. Kumar, S. Lv, D. Xiong, H. Zhao, Z. Cai, X. Zhao, Recent advances in 3D bioprinting of vascularized tissues, Mater. Des. 199 (2021), 109398, https://doi.org/10.1016/j.matdes.2020.109398.
[22] S. Murphy, A. Atala, 3D bioprinting of tissues and organs, Nat. Biotechnol. 32 (2014) 773–785, https://doi.org/10.1038/nbt.2958.
[23] H. Yi, H. Kim, J. Kwon, Y. Choi, J. Jang, D. Cho, Application of 3D bioprinting in the prevention and the therapy for human diseases, Signal Transduct. Target. Ther. (2021) 6, https://doi.org/10.1038/s41392-021-00566-8.
[24] B. Ayan, D. Heo, Z. Zhang, M. Dey, A. Povilianskas, C. Drapaca, I. Ozbolat, Aspiration-assisted bioprinting for precise positioning of biologics, eaaw5111, Sci. Adv. 6 (2020) 5111, https://doi.org/10.1126/sciadv.aaw5111.
[25] A. Gregor, E. Filová, M. Novák, J. Kronek, H. Chlup, M. Buzgo, V. Blahnová, V. Lukášová, M. Bartoš, A. Nečas, et al., Designing of PLA scaffolds for bone tissue replacement fabricated by ordinary commercial 3D printer, J. Biol. Eng. (2017) 11, https://doi.org/10.1186/s13036-017-0074-3.
[26] A. Grémare, V. Guduric, R. Bareille, V. Heroguez, S. Latour, N. L'heureux, J. Fricain, S. Catros, D. Le Nihouannen, Characterization of printed PLA scaffolds for bone tissue engineering, J. Biomed. Mater. Res. Part A 106 (2017) 887–894, https://doi.org/10.1002/jbm.a.36289.